

## Seasonal water and salt cycling in the Great Salt Lake after opening the new causeway breach

Diana Dunn <sup>a,\*<sup>1</sup></sup>, Brian M. Crookston <sup>a,\*<sup>2</sup></sup>, Colin Phillips <sup>a,<sup>3</sup></sup>, Som Dutta <sup>b,<sup>4</sup></sup>,  
Bethany Neilson <sup>a,<sup>5</sup></sup>

<sup>a</sup> Utah Water Research Laboratory, Dept. Civil and Env. Engineering, Utah State University, 8200 Old Main Hill, Logan, UT 84322-8200, USA

<sup>b</sup> Dept. Mechanical and Aerospace Engineering, Utah State University, 8200 Old Main Hill, Logan, UT 84322-8200, USA



### ARTICLE INFO

#### Keywords:

Hypersaline lake dynamics  
Salinity monitoring  
Bi-directional flows  
Adaptive lake management

### ABSTRACT

**Study region:** The Great Salt Lake, the largest saltwater lake in the western hemisphere, located in Utah, USA.

**Study focus:** A railroad causeway divides the Great Salt Lake into north and south arms and significantly alters natural lake dynamics. A new opening in the causeway, referred to as the New Breach, was completed in December 2016 to manage exchange flows between the north and south arms and control salinity primarily in the south arm. Salinity data have been collected independently by multiple stakeholders using different monitoring techniques and instrumentation. To overcome inconsistent data and provide a holistic record of salinity conditions, new methods were developed for curating and compiling all relevant disparate salinity data into a daily representative time series with quantified uncertainties for the south arm of the lake.

**New hydrological insights for the region:** This dataset was used to characterize the altered spatial and temporal patterns of salinity within the south arm during varied hydrologic periods while considering the effects of the New Breach. Results, contextualized by data uncertainties, inform lake management by showing that the New Breach exchange flows influence lake salinity, but the primary controls are related to the balance between river inflows and evaporation. While considering dataset limitations, insights are provided regarding how monitoring at the Great Salt Lake may be improved to better support active lake management efforts.

### 1. Introduction

The Great Salt Lake (GSL), a remnant of ancient Lake Bonneville located in northern Utah, USA, is the largest inland saline lake in North America and the 8th largest in the world (Null and Wurtsbaugh, 2020). It is an important ecological, cultural and economic asset

\* Corresponding authors.

E-mail addresses: [diana.dunn@usu.edu](mailto:diana.dunn@usu.edu) (D. Dunn), [brian.crookston@usu.edu](mailto:brian.crookston@usu.edu) (B.M. Crookston), [colin.phillips@usu.edu](mailto:colin.phillips@usu.edu) (C. Phillips), [som.dutta@usu.edu](mailto:som.dutta@usu.edu) (S. Dutta), [bethany.neilson@usu.edu](mailto:bethany.neilson@usu.edu) (B. Neilson).

<sup>1</sup> ORCID: 0009-0009-6493-6848.

<sup>2</sup> ORCID: 0000-0003-1259-8540.

<sup>3</sup> ORCID: 0000-0001-9950-2497.

<sup>4</sup> ORCID: 0000-0002-9970-0298.

<sup>5</sup> ORCID: 0000-0001-8829-5082.

<https://doi.org/10.1016/j.ejrh.2025.102332>

Received 18 December 2024; Received in revised form 16 March 2025; Accepted 17 March 2025

Available online 10 April 2025

2214-5818/© 2025 The Author(s). Published by Elsevier B.V. This is an open access article under the CC BY license (<http://creativecommons.org/licenses/by/4.0/>).

## Nomenclature

$a_s$	Shuttleworth constant, $a_s = 0.25$
$b_s$	Shuttleworth constant, $b_s = 0.5$
$C$	weir discharge coefficient applicable to broad crested weirs
$c_a$	specific heat of air at constant pressure, $c_a = 1.013 \times 10^{-3}$ [MJ/kg•°C]
$CI_{90\%}$	90 % confidence interval on any given day
$C_{\%S}$	Correction factor for %S conversion, $C_{\%S} = 1.24$ [-]
$d_r$	inverse relative distance Earth-Sun [-]
$E_{GSL}$	evaporative depth off GSL, [m/d]
$e'_s$	saturation vapor pressure of the saline water surface [kPa]
$e_a$	actual vapor pressure of air [kPa]
$E_f$	Nash-Sutcliffe Efficiency [-]
$e_s$	saturated vapor pressure of a freshwater surface at air temperature [kPa]
$G_{sc}$	solar constant, $G_{sc} = 0.0820$ [MJ m <sup>-2</sup> day <sup>-1</sup> ]
$H$	total specific energy or head relative to submerged berm crest [m]
$H_I$	elevation of the exchange flow interface relative to the submerged berm crest [m]
$H_N$	total energy head at the New Breach of the north arm [m]
$H_S$	total energy head at the New Breach of the south arm [m]
$J$	number of day of the year [-]
$K_E$	bulk latent heat transfer coefficient [mm•s/m•kPa•d]
$L$	width of the submerged berm [m]
$M$	total dissolved salt mass flux [metric tons/d]
$M_{NS}$	north to south total dissolved salt mass flux at the New Breach [metric tons/d]
$M_{SN}$	south to north total dissolved salt mass flux at the New Breach [metric tons/d]
$n$	total number of error sources in S
$NS$	north to south
$P$	site pressure [hPa]
$Q$	surface water discharge [m <sup>3</sup> /d]
$Q_{BR}$	Bear River discharge near Corrine, UT [m <sup>3</sup> /d]
$Q_{FB}$	Farmington Bay Bridge discharge [m <sup>3</sup> /d]
$Q_{GD}$	Goggin Drain discharge [m <sup>3</sup> /d]
$Q_{NS}$	north to south discharge at the New Breach [m <sup>3</sup> /d]
$Q_{SN}$	south to north discharge at the New Breach [m <sup>3</sup> /d]
$Q_{WR}$	Weber River discharge [m <sup>3</sup> /d]
$R_a$	extraterrestrial radiation [MJ/m <sup>2</sup> •d]
$R_n$	net energy available at water surface [MJ/m <sup>2</sup> •d]
$R_{nl}$	net outgoing longwave radiation [MJ/m <sup>2</sup> •d]
$R_s$	incoming shortwave solar radiation [MJ/m <sup>2</sup> •d]
$R_{so}$	clear sky solar radiation [MJ/m <sup>2</sup> •d]
$S$	salinity, equivalent to salt concentration [kg/m <sup>3</sup> ≈ g/L]
$\bar{S}$	average salinity [kg/m <sup>3</sup> ≈ g/L]
$SC$	specific conductance [ $\mu$ S/cm]
$SG$	specific gravity [-]
$SN$	south to north
$S_s$	salinity at water surface [g/L]
$T$	temperature [°C]
$TDS$	total dissolved solids
$T_d$	dewpoint temperature of air [°C]
$T_a$	mean air temperature [°C]
$T_{a,max}$	maximum daily air temperature [°C]
$T_{a,min}$	minimum daily air temperature [°C]
$T_{max,K}$	maximum daily air temperatures [°K]
$T_{min,K}$	minimum daily air temperatures [°K]
$T_s$	air temperature at the water surface [°C]
$V$	volume of the sample [mL]
$\alpha$	shortwave radiation reflection coefficient, $\alpha = 0.08$ [-]
$\beta$	water activity coefficient
$\gamma$	psychrometric constant [kPa/°C]

$\Delta'$	saturation vapor pressure gradient [kPa/ $^{\circ}$ C]
$\delta$	solar declination [rad]
$\lambda_v$	latent heat of evaporation [MJ/kg]
$v_w$	wind velocity at water surface [m/d]
$\pi$	geometric constant Pi [-]
$\rho$	density of water [g/cm <sup>3</sup> , kg/m <sup>3</sup> ]
$\rho^0$	density of pure water [g/cm <sup>3</sup> , kg/m <sup>3</sup> ]
$\rho_{20}$	density of water at 20 $^{\circ}$ C [g/cm <sup>3</sup> , kg/m <sup>3</sup> ]
$\rho_N$	density of the north arm brine [kg/m <sup>3</sup> ]
$\rho_S$	density of the south arm brine [kg/m <sup>3</sup> ]
$\sigma$	Stefan Boltzmann constant, $\sigma = 4.903 \times 10^{-9}$ [MJ K <sup>-4</sup> m <sup>-2</sup> day <sup>-1</sup> ] or daily standard deviation [g/L]
$\sigma_1^2 - \sigma_n^2$	average variance of each error source during the period of analysis [g <sup>2</sup> /L <sup>2</sup> ]
$\sigma_T$	total standard deviation [g/L]
$\varphi$	latitude [rad]
$\omega_s$	sunset hour angle [rad]
%S	percent salinity [%]
% $\varepsilon$	measurement uncertainty

yet has experienced reduced biodiversity, altered salinity composition and limnology, and desiccation due to human activity ([ECONorthwest, 2019](#)). An east-west rockfill railroad causeway was constructed in 1959 that segregated the lake into north and south arms (sections), resulting in the north arm having no freshwater inflows. It featured two culverts to facilitate water and salt mass exchange between the arms; however, distinct water surface elevation and density gradients have formed causing salinity, ecologic community structure, and nutrient dynamics to differ between the two arms of the lake.

Despite alterations to its natural state, the lake supports a productive endemic ecosystem with brine shrimp, brine flies, various phytoplankton, and benthic microbial communities residing in the less saline south arm ([Brown et al., 2023](#)). Large avian populations use the GSL for breeding and migration and it is one of a limited number of wetland sites within North America's Pacific Flyway ([Donnelly et al., 2020](#); [Yang et al., 2020](#)). Brine shrimp cysts are harvested from the south arm and used as food sources for global commercial aquaculture operations. The lake is estimated to contain 90 billion USD in minerals, which are extracted from the hypersaline brine and utilized for various salt-containing products, metal alloys, fertilizer, and in the production of glass and paper ([Bioeconomics, 2012](#)).

During the past 50 years the GSL has experienced significant lake level fluctuations. Periodic droughts combined with upstream water withdrawals for agriculture have resulted in record high salt concentrations ([Null and Wurtsbaugh, 2020](#), [Williams et al., 2020](#)). These conditions have threatened brine shrimp and other organisms ([Barnes and Wurtsbaugh, 2015](#); [Lindsay et al., 2019](#)) and caused a loss of habitat for water and shorebird populations ([Wurtsbaugh, 2014](#)). Lake fluctuations have also caused millions of dollars in economic damage, primarily to the brine shrimp cyst harvesting and mineral extraction industries ([ECONorthwest, 2019](#)). Dry sections of now exposed lakebed result in wind erosion which mobilizes dust that poses a significant human health risk for the 2.7 million residents of the Salt Lake City metropolitan area 20 kilometers east of the GSL ([Perry et al., 2019](#)).

Multiple strategies have been identified to increase lake levels and manage salinity including water conservation focused on agricultural optimization ([Great Salt Lake Strike Team, 2024](#)). However, historically, engineered solutions have been the predominant management approach. For example, in December 2016 a 55 m breach, referred to as the New Breach, was opened to facilitate exchange flows through the causeway to minimize differences in water level between the north and south arms ([HDR Engineering, Inc., 2014](#)). The New Breach also features a submerged rock berm that can be raised or lowered to manage salt export from the highly saline north arm to the south arm ([Rasmussen et al., 2021](#)). The height of the New Breach berm has been raised multiple times since it was opened in response to changing hydroclimatic conditions that altered the spatial and temporal distribution of salinity within the lake.

Salinity monitoring throughout the south arm has been conducted by various stakeholders to assess lake response to the breach and associated berm management decisions. Prior to 2020 there was limited coordination across entities regarding field and analytical methods due to varying monitoring goals. The [Great Salt Lake Salinity Advisory Committee \(2020a\)](#) summarized available datasets and developed a standard operating procedure for future monitoring. However, they did not analyze how to effectively utilize historical data, which includes salinity data derived from multiple water quality parameters. This prevents a comprehensive understanding of the changing lake conditions post-breath opening and allows only subsets of the available data to be used to guide future management strategies.

Despite the disparate data, various studies have aimed to determine how breach related management decisions have altered the lake. [Yang et al. \(2020\)](#) quantified density stratification in the south arm, attributing changes in the deep brine layer (DBL) to New Breach exchange flows and hydrologic conditions based only on density data from the U.S. Geological Survey (USGS) from a limited number of sites in the south arm. [Jewell \(2021\)](#) developed a mass balance model that provided further insight into the drivers of density stratification, comparing the magnitude of New Breach exchange flows to causeway subsurface flux. However, rather than capturing the New Breach impacts, this model relied on an old model of culvert flow exchange and only considered monthly density measurements from a subset of USGS and Utah Geological Survey (UGS) south arm sampling locations. [Merck and Tarboton \(2023\)](#) evaluated how historical management actions over a longer time period have affected the distribution of total dissolved salt mass through the water column and between arms of the lake. [Brown et al. \(2023\)](#) also expanded the understanding of salt movement and

partitioning within the lake, using interpolated measurements of New Breach flow and south arm salinity data to chronicle and quantify salt flux through the causeway since opening of the New Breach. Nevertheless, Brown et al. (2023) relied only on bi-weekly salinity data collected at two south arm sites and monthly or bi-monthly New Breach flow measurements while Merck and Tarboton (2023) only used density data.

While informative, these studies have had to rely on limited datasets and were unable to analyze the combined influences of the New Breach and varying hydrologic conditions on seasonal salinity changes throughout the south arm upper brine layer (UBL). Knowledge of the key drivers of salinity within the UBL influences future monitoring and management decisions, therefore, the primary objectives of this study are to: 1) develop methods for creating a comprehensive salinity record for the GSL post New Breach opening, 2) analyze this data to establish the critical drivers of UBL salinity variability, and 3) evaluate the efficacy of historical salinity management strategies.

## 2. Study area

The Great Salt Lake is in a semi-arid climate with inflows primarily provided to the south arm via three rivers and their corresponding subbasin drainage areas (Fig. 1). As a closed-basin lake, it is sensitive to climate variability where fluctuations in lake water surface and volume are determined by the balance between evaporation and water inflows (river discharge, precipitation, surface runoff and groundwater seepage) (Wang et al., 2010). Water is diverted from GSL's main tributaries for agricultural and metropolitan consumptive use which influences the lake's natural hydrologic balance and compounds the effects of long-term periods of drought.

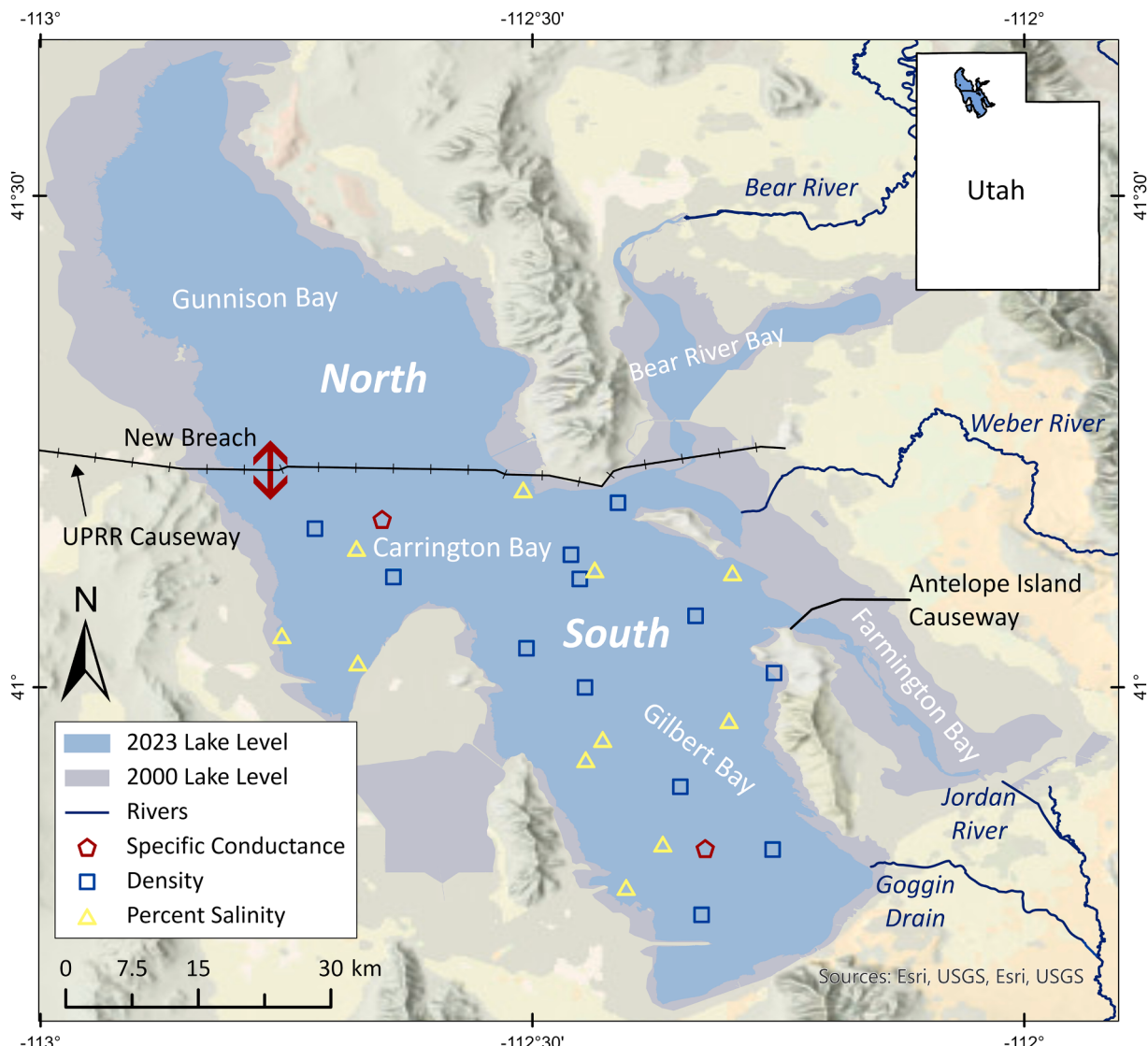


**Fig. 1.** Location and key features of the Great Salt Lake including its bays, tributaries, and the New Breach.

Seasonality also affects GSL elevation, which normally fluctuates less than 1 m per year. Lake levels typically rise November to June due to direct precipitation and spring runoff (snowmelt) and decrease from July to October due to warmer temperatures and a dry climate (Fig. 2).

Prior to anthropogenic influence, lake salinities ranged from 60 to 330 g per liter (g/L) but generally less than 200 g/L (Null et al., 2013). The east-west rockfill railroad causeway divides the lake (Fig. 1) into the north arm (Gunnison Bay) and the south arm (comprised of Gilbert and Carrington Bay) (Marden et al., 2020). The lake is further partitioned by a vehicle roadway segregating Farmington Bay in the southeast corner of the lake. Currently, the north arm has salt concentrations near saturation, around 330 g/L, while salt concentrations south of the causeway fluctuate from 50 to 180 g/L (Wurtsbaugh, 2014; Fig. 1). Elevation and density gradients between the segregated arms of the lake are present because river inflows only enter the south arm which is commonly 0.3–0.6 m higher in elevation than the north arm. Furthermore, the south arm features two well defined intermittent brine layers, the UBL and the DBL (Madison, 1970). The DBL is formed by the higher salinity north arm waters passing through the causeway and plunging below the less saline UBL (Naftz et al., 2014). This DBL dissipates without northern water inflows or with high winds across the GSL that cause significant mixing events.

Alterations to the causeway have occurred periodically for various reasons. For many years, two box culverts allowed for limited mass exchange between the two arms. In 1984, an additional breach was added on the far west side of the causeway, known as the Lakeside Breach, to alleviate urban flooding and reduce the 1.5 m rise in the south arm lake elevation (Gwynn and Sturm, 1986). However, due to drought and historically low lake levels in the 2000s, the Lakeside Breach has been ineffective in exchanging flows (Jewell, 2021). The culverts were decommissioned in 2013 and 2014 since they subsided into the lakebed and deteriorated (White and Null, 2015). To once again provide exchange flows between the north and south arms, the New Breach was constructed with completion December 2016 (see Section 2, Appendix B) that featured a submerged berm to control movement of hypersaline north brine to the south arm. In July 2022, the berm was raised from elevation 1275 m to elevation 1276.2 m, reducing north to south (NS) flow and corresponding salt mass loading to the south arm. Prior to the 2023 spring runoff, the berm was raised above current lake elevations to 1277.7 m to limit flow and salt exchange and lower south arm salinities (Fig. 2). However, high spring runoff increased water levels in the south arm and overtopped the berm, reestablishing south to north (SN) flow.

In summary, the New Breach successfully reestablished exchange flows while raising the height of the berm was performed as an adaptive measure to combat the effects of declining annual average lake levels which have occurred since its construction. The GSL reached a record low of 1276.7 m in November 2022 due to decreased streamflow reaching the lake and the recent megadrought sustained across the southwest United States (Great Salt Lake Strike Team, 2023; Fig. 2). Salinity values that exceed optimal range for ecosystem health (> 160 g/L) have been recorded since 2021, emphasizing the need to better understand the primary drivers of salinity in the UBL for sustainable management of the GSL and its watershed (Great Salt Lake Salinity Advisory Committee, 2021; Brown et al., 2023).

### 3. Methods

To further detail the methods and supporting data used in this study, additional information regarding climate and exchange flow data is provided in Appendix A. Furthermore, a method flow chart (Fig. S1, Appendix B) and supporting calculations and analyses, including laboratory and field data, are provided in Appendix B.

#### 3.1. Data collection and compilation

Data pertaining to the opening of the New Breach (Fig. S2, Appendix B) began January 2017. Since then, multiple entities have gathered and reported various hydrologic and salinity data for the GSL (Table 1; Table A1–A2; Fig. S3, Appendix B) including the Utah Geological Survey (UGS); the US Geological Survey (USGS); Utah Division of Wildlife Resources (DWiR); Henningson, Durham and

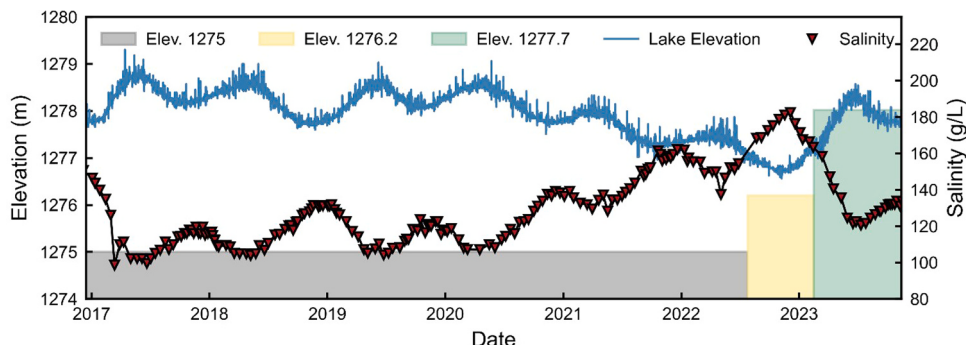


**Fig. 2.** Gilbert Bay water surface elevation from USGS site 10010000 and salinity from DWiR site 3510. Gray shaded region represents the New Breach berm at elevation 1275 m, the yellow shaded region represents the New Breach berm at elevation 1276.2 m and the green shaded region represents the New Breach berm at elevation 1277.7 m.

Richardson, Inc. (HDR); the Great Salt Lake Brine Shrimp Cooperative (BSC); and Utah State University (USU) ([Great Salt Lake Salinity Advisory Committee, 2020a, 2020b](#)). Different measures of salinity from these five entities needed to be compiled into a single dataset. This required determining appropriate methods for converting various measurements from these entities to salinity,  $S$  (g/L). To do this, a new conversion equation for specific conductance,  $SC$  ( $\mu\text{S}/\text{cm}$ ), had to be established since the existing published conversion methods had not been developed for hypersaline environments. Once the  $S$  datasets were compiled, additional hydrologic data, including New Breach exchange flows, stream flows, and climate variables, were gathered to quantify water and salt mass fluxes for use in exploring seasonal controls on south arm  $S$ .

### 3.1.1. South arm open water salinity

During the period of analysis, USGS measured south arm water sample  $\rho$ , temperature,  $T$  ( $^{\circ}\text{C}$ ), and  $SC$  for 8 sites in the south arm and at the New Breach ([Table 1](#); [Fig. S3, Appendix B](#)), which was compiled from the National Water Information System (NWIS) ([U.S. Geological Survey, 2023](#)). UGS measured  $\rho$ ,  $T$ , and ion composition at 5 sites in the south arm. This data was compiled from the Brine Chemistry database available through the UDWQ ([Utah Geological Survey, 2020](#)). HDR Engineering measured  $\rho$  and  $SC$  at 5 sites in the south arm and at the New Breach. Reported HDR data pertained to the GSL Causeway Culvert Closure and Bridge Construction Project were accessed through UDWQ ([Utah Department of Water Quality, 2022](#)). DWiR collected percent salinity,  $\%S$ , data at 16 sites only in the south arm ([Great Salt Lake Salinity Advisory Committee, 2020a](#)) while BSC reported  $S$  at two sites in the south arm ([Brown et al., 2023](#)).

DWiR, as part of the GSL Ecosystem Program (GSLEP), sampled  $\rho$  at four measurement sites 0.2–0.5 m below the lake surface and 0.5 m above the lake bottom and provided these samples to USGS for analysis. USGS collected and analyzed samples at 8 other locations ([Table 1](#)); GSLEP and USGS samples were analyzed at the USGS laboratory following published protocols ([Great Salt Lake Salinity Advisory Committee, 2020b; U.S. Geological Survey, 2002](#)) with  $\rho$  values adjusted to  $20^{\circ}\text{C}$  equivalent values. UGS sampled  $\rho$  near the water surface, at 1.5 m intervals, and just above the lake bottom. Samples were also analyzed at a commercial lab for ion composition ([Great Salt Lake Salinity Advisory Committee, 2020a, 2020b](#)). HDR analyzed samples for  $\rho$  at the water surface, in 1.5 m descending intervals, and 0.3 m from the lake bottom ([Utah Department of Water Quality, 2022](#)). USGS, UGS, and HDR report an accuracy of  $\pm 0.001 \text{ g/cm}^3$  for all  $\rho$  measurements ([Great Salt Lake Salinity Advisory Committee, 2020a](#)).

USGS datasets included  $SC$  measured in the field at the water surface, at 1 m intervals, and near the lake bottom using a calibrated multiparameter sonde ( $\pm 5\%$ ). HDR measured vertical profiles of  $SC$  in the field using an In-Situ Aqua TROLL multiprobe water quality meter ( $\pm 0.8\%$ ) where depth intervals included every 10 cm for the first meter, every 0.3 m from 1 m down to the beginning of the DBL, and every 15 cm in the DBL. BSC also conducted vertical profiling, measuring  $S$  at 1, 3, 5, 6, 7, and 8 m depths using a YSI-556 conductivity meter which converts  $SC$  to  $S$ . BSC then corrected profile measurements to  $\%S$  field measurements using a regression equation ([Brown et al., 2023](#)). Current  $SC$  conversion equations ([Schemel, 2001](#)) have an upper limit of 50 g/L, significantly lower than  $S$  observed at the GSL, thus a new conversion equation was developed and used herein (see [Section 3.2](#)). Finally, DWiR collected  $\%S$  data at the water surface using a refractometer with an accuracy of  $\pm 0.2\%$ .

Since this study focused on the open water portion of the south arm UBL, a sensitivity analysis of the combined data set was conducted to determine if the lake could be considered as a single UBL volume or if spatial volume partitioning was needed.

### 3.1.2. New Breach salinity

From August 2020 to February 2022, Utah State University's Utah Water Research Lab (UWRL) collected nearly continuous 15-minute  $SC$  data and monthly water samples taken at the New Breach as part of the field campaign outlined in [Rasmussen \(2022\)](#) ([Table A1](#)). The 15-minute continuous  $SC$  data was collected using two In-Situ AquaTroll 600 Multiparameter Sondes placed on the north and south sides of the New Breach ([Fig. S2a, Appendix B](#)). Due to dropping lake elevations during the recent drought, these instruments were relocated from February 2022 to February 2023 to a vertical slotted casing attached to a pier on the north side of the bridge ([Fig. S2b, Appendix B](#)) directly south of the berm, with instruments placed at an elevation of 1272.7 m (in the DBL near the bottom of the water column) and at 1277 m (in the UBL at the middle of the water column) ([Dunn, 2024](#)). North and south arm water

**Table 1**  
Open water  $S$  datasets.

Entity	Parameter Reported	Number of South Arm Sites	Measurement Type	Frequency	Depth	Period of Record (Yr./Mo/Day)
USGS	$SC$ ( $\mu\text{S}/\text{cm}$ )	13	in-field	twice a year	0.3 m increments	2017/1/1–2022/12/31
	$\rho$ ( $\text{g}/\text{cm}^3$ )	9	sample	monthly, bi-monthly	0.2–0.5 m below surface, 0.5 m above bottom	
	SG					
UGS	$\rho$ ( $\text{g}/\text{cm}^3$ )	5	sample	4 months	1.5 m below surface, 0.15 m from bottom	2017/1/1–2022/5/23
DWiR	$\%S$	16	sample	2 weeks	at water surface	2017/1/1–2022/12/31
	$SC$ ( $\mu\text{S}/\text{cm}$ )				0.15–0.3 m increments	
HDR	$\rho$ ( $\text{g/mL}$ )	6	in-field	3 months	at surface, 1.5 m increments, 0.3 m above bottom	2017/1/1–2021/12/1
	$S$ (g/L)	2	in-field	monthly	1, 3, 5, 6, 7 and 8-m	
*BSC						2017/1/1–2021/11/4

\* BSC reports  $S$  in g/L computed by a YSI 556 conductivity meter using conductivity and  $T$  readings in-situ.

samples were also collected monthly and analyzed at the Utah Water Research Lab (UWRL) for  $\rho$  and total dissolved solids, TDS (g/L) (Rasmussen, 2022).

### 3.1.3. New breach exchange flows

Flows through the New Breach are a significant challenge to estimate due to 1) observed daily fluctuations and lack of high frequency discrete discharge measurements, 2) the high salinity and water density difference across the New Breach that results in the commonly occurring buoyancy-driven bi-directional flow pattern, and 3) the geometry of the New Breach and periodic adjustment in height to the submerged berm. To consider these challenges, several new models were developed to predict SN and NS discharge,  $Q$  ( $\text{m}^3/\text{s}$ ), as formulated by Larsen (2024) and detailed in Appendix B (Section 3). A deep neural network (DNN) model was developed to predict 15-minute  $Q$  estimates for the 1275 m berm case and a Generalized Area Based Index (GABI) model for the 1276.2 m berm case.

DNN model data inputs consisted of the USGS Acoustic Doppler Velocity Meter (ADVM) up-looker data (a velocity profile sampled at 15- minute frequency) that included velocities in 10 equidistant cells. Due to a blanking distance (no observed velocity near the bottom of the New Breach), an 11th cell was added to complete the velocity profile and mimic a no slip boundary (Fig. S4, Appendix B). The DNN model output was informed by  $Q$  estimated by a provisional index velocity rating curve (Levesque and Oberg, 2012) developed by USGS for exchange flows at the New Breach.

The GABI model is similar in principle to the DNN model as it is based upon the USGS up-looker velocity data. However, it considers the 1276.2 m berm raise and three distinct flow cases: bi-directional flow and either SN or NS unidirectional flow. It was necessary to develop the GABI model because there were not sufficient discrete flow measurements available for the 1276.2 m berm scenario to train the DNN. Thus, GABI uses the measured velocity and the known area of the cross-section to estimate the NS and SN flow through the breach. To accomplish this, Larsen (2024) estimated the vertical location of any interface,  $H_l$ , between  $Q_{NS}$  and  $Q_{SN}$  via a hydrostatic analysis based upon the difference between lake elevations and  $\rho$  on either side of the New Breach, referencing the top of the berm (note that the USGS ADVM does not identify the exact interface location due to the 11-cell approach for the vertical velocity profile). The available ADVM measurements were assigned to the vertical midpoint of each cell with linear interpolation used between cells. This interface location and augmented vertical velocity profile is then used to estimate  $Q$ .

A daily time series of New Breach  $Q_{NS}$  and  $Q_{SN}$  was developed utilizing monthly discrete  $Q$  measurements from USGS supplemented with 15-minute incremental  $Q$  outputs from the DNN and GABI models (for validation see Fig. S5 and S6, Appendix B). From January 2017 to July 2017, the monthly USGS discrete measurements were linearly interpolated for daily  $Q$ . From July 2017 to July 2022, a daily average of the 15-minute DNN model  $Q$  was used and from August 2022 to December 2022, the GABI model  $Q$  outputs were used.

### 3.1.4. River Inflows

USGS measured continuous stream flow to the south arm of the GSL at Farmington Bay Bridge (FB); Weber River (WR) at Plain City, UT; Goggin Drain (GD); and the Bear River (BR) near Corinne, UT (U.S. Geological Survey, 2023; Table A1; Fig. S3, Appendix B). Continuous  $Q$  records from these four major tributaries were gathered from the NWIS database using the data retrieval package in Python (U.S. Geological Survey, 2023; Horsburgh et al., 2022; Table A1).

### 3.1.5. Climate

Continuous hourly climatic data was available at three sites in the Great Salt Lake from the Utah Climate Center (UCC), managed by Utah State University (Utah State University, 2024). Hourly dewpoint temperature,  $T_d$  ( $^\circ\text{C}$ ), wind velocity,  $v_w$  (m/s), and site pressure,  $P$  (hPa), since 2017 was gathered along with daily maximum and minimum air temperature,  $T_{a,max}$  and  $T_{a,min}$  ( $^\circ\text{C}$ ) (Table A2; Fig. S3, Appendix B). The USGS also measured 15-minute  $v_w$  at the New Breach, which was compiled from the USGS NWIS database.

## 3.2. Data curation

### 3.2.1. Evaluation of great salt lake salinity

As noted, the various available datasets summarized in Table 1 used different field methods to collect water quality data for use in estimating  $S$ , necessitating appropriate conversion methods for hypersaline environments. In this study, the north arm and south arm water quality data from each entity was converted to  $S$  in g/L and compiled into the GSL dataset (Dunn, 2025). Data pertaining to the south arm was apportioned to either the UBL or the DBL using a depth to DBL dataset developed by the USGS, which utilized profile measurements from only two sites, Carrington Bay and Gilbert Bay (McIlwain et al., 2023). Direct  $\rho$  measurements were prioritized in this analysis due to  $\rho$  being the most common measurement across agencies (Great Salt Lake Salinity Advisory Committee, 2020a, 2020b).

To convert  $\rho$  to  $S$ , an equation of state (EOS, see Eq. (1)) derived specifically for the GSL for  $S$  ranging from 0 to 180 g/L and for  $T$  ranging from 4 to 50  $^\circ\text{C}$  was applied (Naftz et al., 2011):

$$\rho - \rho^0 = 184.01062 + 1.04708S - 1.21061T + 3.14721 - 4S^2 + 0.00199T^2 - 0.00112ST \quad (1)$$

where  $\rho$  is measured density of GSL water ( $\text{g}/\text{cm}^3$ ),  $T$  is in ( $^\circ\text{K}$ ), and  $S$  is in ( $\text{g}/\text{L}$ ).  $\rho^0$  is the density of pure water at the sample temperature ( $\text{g}/\text{cm}^3$ ) calculated using Eq. (2) (Spieweck and Bettin, 1992):

$$\rho^0 = [999.83952 + 16.952577(T - 273.15) - 7.9905127 - 3(T - 273.15)^2 - 4.6241757 - 5(T - 273.15)^3 + 1.0584601 - 7(T - 273.15)^4 - 2.8103006 - 10(T - 273.15)^5] / [1 + 0.016887236(T - 273.15)] \quad (2)$$

which is regularly used by Utah DNR and was extended by the USGS for  $S \leq 275$  g/L and current GSL conditions (Mcilwain et al., 2023). Note that  $\rho$  varies with  $T$  yet each entity measures  $\rho$  at different temperatures. For this study, all  $\rho$  samples not measured at  $T = 20$  °C, including data from HDR and UGS, were converted before being used in Eq. (1). Eq. (3) is specifically for the GSL:

$$\rho_{20} = \rho + 0.0004417(T - 20) \quad (3)$$

where  $\rho_{20}$  is the estimated sample density at 20 °C (g/cm<sup>3</sup>) and  $T$  is in (°C).

The American Water Works Association (AWWA) developed Eq. (4) to convert SC to  $S$  (Schemel, 2001):

$$S = K_1 + K_2 R^{0.5} + K_3 R + K_4 R^{1.5} + K_5 R^2 + K_6 R^{2.5} \quad (4)$$

where  $S$  is in practical salinity units (psu), the coefficients  $K_1 = 0.0120$ ,  $K_2 = -0.2174$ ,  $K_3 = 25.3283$ ,  $K_4 = 13.7714$ ,  $K_5 = -6.4788$ ,  $K_6 = 2.5842$ , and  $R$  is calculated to be:

$$R = \frac{SC_{sample}}{SC_{seawater}} \quad (5)$$

with  $SC_{sample}$  equal to  $SC$  of the water sample at 25 °C in (μS/cm) and  $SC_{seawater}$  equal to  $SC$  of standard seawater at 25 °C (53,087 μS/cm). However, this equation is only valid for 2 g/L  $\leq S \leq 50$  g/L whereas recorded values of GSL brine from 2017 to 2023 were as high as 300 g/L. An equation to convert  $SC$  of hypersaline brine to  $S$  was not available. Therefore, a new conversion equation, Eq. (6), was developed in this study at the Environmental Quality Laboratory (EQL) in the UWRL at USU for 20 g/L  $\leq S \leq 290$  g/L (Dunn, 2024; Section 4, Appendix B) where  $SC$  is in (μS/cm):

$$SC = (-3.85 \times 10^6)\rho_{20}^2 + (9.48 \times 10^6)\rho_{20} - 5.61 \times 10^6 \quad (6)$$

In the EQL, a laboratory solution of brine with  $S = 300$  g/L and the same ion composition as the Great Salt Lake was prepared (Fig. S7, Appendix B).  $\rho$  was directly measured by removing a subsample with volume,  $V$ , and measuring total mass of the subsample,  $M$ , with  $\rho = M/V$ . As with in-situ field measurements, the laboratory solution was also measured for  $SC$  (μS/cm) and  $T$  (°C) with the In-Situ Aqua Troll 600 series water quality sonde. %S of the sample was also measured using an Atago MASTER-S28a refractometer. Solutions of 20 g/L  $\leq S \leq 290$  g/L were prepared by diluting and thoroughly mixing the original solution for twenty separate water samples. The performance of Eq. (1), Eq. (4) and Eq. (6) to calculate  $S$  via the USU-UWRL dataset was plotted as a function of  $\rho$  and considered via calculated Mean Absolute Percent Error (MAPE) values (see Section 4.1). The EQL experiment data was also used to evaluate the conversion between %S to  $S$  (g/L) using Eq. (7) (Chapra, 1997):

$$S = C_{\%S} \times \%S \times \frac{1}{100} \times \rho \quad (7)$$

where  $\rho$  is in (kg/m<sup>3</sup>). When compared to the  $\rho$  method, Eq. (7) was found to overestimate  $S$  so a correction factor,  $G_{\%S}$ , was developed by plotting the %S method against the  $\rho$  method for each sample and computing the slope of the linear regression line. This correction was applied to all the DWiR observations within the compiled salinity dataset. While USU-UWRL sample  $T$  recordings were within a small range, 20–23 °C, all  $\rho$  measurements were standardized to 20 °C via Eq. (3) to minimize any potential variability in  $\rho$  due to  $T$  differences between samples.

### 3.2.2. New Breach salt flux

To calculate NS and SN New Breach salt flux,  $M$  (metric tons/d), for use in the principal component and correlation analysis,  $S$  from both USGS and HDR New Breach samples (January 2017–August 2020) were used. Also included in this analysis were the USU 15-minute continuous  $S$  record (August 2020–December 2022) and the USU New Breach  $Q$  dataset (January 2017–December 2022). Any gaps in the  $S$  record at the New Breach were linearly interpolated to pair with the 15-minute continuous  $Q$  dataset. New Breach  $M$  was calculated separately for NS and SN flow through the New Breach using (Chapra, 1997):

$$M = QS \quad (8)$$

where  $M$  is in (metric tons/d),  $Q$  is in (m<sup>3</sup>/d), and  $S$  is in (metric tons/m<sup>3</sup>).

### 3.2.3. Evaporation

A daily arithmetic average was applied to the hourly climate data at each site (Table A2). These daily values were spatially averaged to produce a single daily time series for each variable for the GSL. The representative climatic data and a modified version of the Penman equation was used to calculate depth of evaporation ( $E_{GSL}$ ) off the GSL at each salinity sampling location (Mohammed and Tarboton, 2012):

$$E_{GSL} = \frac{\Delta'}{\gamma + \Delta'} \bullet \frac{R_n}{\lambda_v \rho_w} + \frac{\gamma}{\gamma + \Delta'} \bullet K_E v_a(e_s(T_a)\beta(T_a, S) - e_a(T_d)) \quad (9)$$

where  $E_{GSL}$  is in (m/d),  $\Delta'$  is the saturated vapor pressure gradient for a saline surface (kPa/°C),  $\gamma$  is the psychrometric constant

(kPa/°C),  $R_n$  is the net energy available at the water surface (MJ/m<sup>2</sup>•d),  $\lambda_v$  is the latent heat of evaporation (MJ/kg),  $\rho_w$  is density of water (kg/m<sup>3</sup>),  $K_E$  is the bulk latent heat transfer coefficient approximated to be  $1.28 \times 10^{-3}$  (ms/(m•kPa•d)) (Mohammed, 2006),  $v_a$  is wind velocity at the water surface (m/d),  $e_s$  is saturated vapor pressure of a freshwater surface at air temperature (kPa),  $e_a$  is actual air vapor pressure at dewpoint temperature (kPa),  $\beta$  is the water activity coefficient,  $T_a$  is mean daily air temperature (°C),  $T_d$  is mean daily dewpoint temperature (°C), and  $S$  is salinity of the GSL water (g/L). Additional details regarding evaporation calculations are provided in Appendix B (Section 5).

### 3.3. Principal component analysis

The New Breach was constructed to aid management of south arm UBL  $S$ , yet the spatial and seasonal influence of New Breach  $M$  compared to other influential variables is not well understood. Therefore, a principal component analysis, PCA (Helsel et al., 2020), was performed to explore the spatial and seasonal patterns of UBL  $S$  since opening of the New Breach. The PCA was performed using the SciKit-Learn package in Python (Vanderplas, 2016). Discrete south arm open water  $S$  observations from the UBL were paired with daily averages of  $E_{GSL}$ ,  $M_{NS}$ ,  $M_{SN}$  and  $Q$  from lake inflows. Due to limited temporal data, open water sites with at least three water samples per year over three consecutive years during the period of analysis were included to retain seasonality in the dataset. For sites where a water quality profile was reported,  $S$  profiles above the DBL interface (Mcilwain et al., 2023) were averaged to represent the UBL as a daily average at the time of sampling.  $M_{NS}$ ,  $M_{SN}$ , FB, BR, WR, and GD  $Q$  were included as separate variables in the PCA. Groundwater and precipitation (arid, local annual average of 472 mm) contributions to the lake were not included based upon unmeasured groundwater flow to the lake and the hydrologic analysis of the GSL by Mohammed and Tarboton (2012), which found these parameters to be negligible.

In this study, data seasonality and exploratory PCA results merited a three-season PCA application: spring during snowmelt and high runoff (RO) between March and June, summer and fall where air temperatures are typically hot with low river inflows (hot low flow, HLF) between July and October, and winter when temperatures are lowest accompanied by low river inflow (cold low flow, CLF) between November and February. Since a PCA is sensitive to outliers and the differing variable magnitudes, histograms and descriptive statistics were compiled for the datasets used in the PCA (Appendix B, Section 6). Any variable that demonstrated a skewed distribution was log-transformed and all variables were standardized before performing the analysis.

### 3.4. Representative south arm salinity

When examining the GSL south arm UBL  $S$  dataset, a small subset of measurement sites exhibited daily deviations likely due to topographic effects (wind, lake circulation, etc.) and any routine mineral extraction activities. Therefore, results from the PCA were used to assist with data filtering where seasonal outliers were removed to reveal a clear central trend in  $S$  within the dataset. A daily, south arm UBL  $S$  time series was then calculated by 1) preparing daily time series of  $S$  at each sampling location, with supplemental temporal data estimated through linear interpolation, then 2) determining the daily median value across sampling locations. Since the filtered dataset revealed a strong central trend, this daily time series is presumed to be representative of general south arm conditions.

Measurement uncertainty compounded by multiple independent data sets, the conversion to  $S$ , spatial averaging of  $S$ , and linear interpolation to fill missing temporal data were of great concern when developing the south arm  $S$  time series. Therefore, to gain greater insight into these uncertainties and given the simplification of spatial homogeneity in this study, the filtered UBL  $S$  data was segregated into measurements derived from  $\rho$ ,  $SC$  and  $\%S$ . The daily standard deviation,  $\sigma$  (g/L), for each parameter was calculated and the average used as a metric regarding spatial uniformity for the GSL. Two additional subsets were taken from the  $S$  data: one including observations from sites B and L and another with observations from sites E and K (Fig. S3, Appendix B). These additional subsets encompassed sampling locations from BSC, DWIR, and USGS that were closest in proximity to each other and were used to quantify uncertainty in combining  $S$  data from multiple datasets. Measurement uncertainties due to instrumentation accuracy, as reported by manufacturer documentation, were also referenced. Additional quantification of measurement uncertainties by various entities and their field programs was not considered herein.

In this study these sources of uncertainty were assumed to be uncorrelated. Total standard deviation,  $\sigma_T$  (g/L), for the representative  $S$  time series was calculated using a first order error analysis approach (Brown and Hambley, 2002):

$$\sigma_T = \sqrt{\sum_{i=1}^n \sigma_1^2 + \sigma_2^2 + \sigma_3^2 + \dots + \sigma_n^2} \quad (10)$$

where  $n$  is the total number of error sources and  $\sigma_1^2$ ,  $\sigma_2^2$ ,  $\sigma_3^2$ ,  $\sigma_n^2$  (g<sup>2</sup>/L<sup>2</sup>) are the average variance associated with each error source during the period of analysis. A 90% confidence interval for the median UBL  $S$  time series was then calculated assuming a normal  $S$  distribution:

$$CI_{90\%} = \bar{S} \pm 1.65\sigma_T \quad (11)$$

where  $CI_{90\%}$  is the 90 % confidence interval and  $\bar{S}$  is average UBL salinity (g/L) on any given day during the period of analysis.

### 3.5. Seasonal salinity drivers

The seasonal influence of each forcing variable on the representative south arm  $S$  time series was investigated by performing a

regression analysis using the non-parametric Theil-Sen method, which is resistant to outliers and represents the median regression line. The regression was performed on the log-transformed data used in the PCA (subset for water year 2020) and further segregated into RO, HLF, and CLF seasons. The entire time series was not selected since an initial analysis showed the magnitude of salinity values within each season fluctuated across years and formed data clusters within the analysis period. To clarify the results, data from water year 2020 was selected as it exhibited average hydroclimatic conditions compared to the entire period of analysis. The 95 % confidence intervals surrounding the calculated Theil-Sen slopes were determined and used to evaluate the significance of the linear relationships between log transformed  $S$  and  $E_{GSL}$ ,  $M_{SN}$ ,  $M_{NS}$ , and river  $Q$  across seasons.

## 4. Results

### 4.1. Data curation and characterization

Performance of Eq. (6) showed validity for  $\rho$  up to  $1.25 \text{ g/cm}^3$  (Fig. 3a). The water samples prepared at the USU UWRL EQL and the USGS samples taken at the New Breach were in close agreement and followed the same nonlinear trend. The USGS data exhibited significant measurement uncertainties ( $\%e$ ) for  $\rho \geq 1.2$ . This can be attributed to field uncertainties because the USU laboratory experiment required significant mechanical mixing to achieve sample uniformity at these salt concentrations. Mean absolute percent errors (MAPE) of the AWWA conversion (Eq. (4)) when compared to Naftz EOS (Eq. (1)) was 10.1 % while MAPE of Eq. (6) was 3.3 %. The performance difference is due to the original range of  $S$  used to formulate the AWWA method (Schemel, 2001), as good agreement exists for  $\rho < 1.1 \text{ g/cm}^3$ . However, prediction uncertainties via Eq. (4) increased for  $\rho \geq 1.1 \text{ g/cm}^3$ . The correction constant  $C_{\%S} = 1.24$ , based upon the relationship between  $S$  measured in the laboratory and  $S$  predicted via Eq. (7), indicated that  $\%S$  measurements at the GSL tended to overestimate  $S$  when compared to  $\rho$  measurements (Fig. 3c). The DWiR dataset, based upon a refractometer, was adjusted accordingly herein.

The histograms, descriptive statistics and time series prepared for exploratory analysis preceding the PCA provided insight into the magnitude and frequency of key variables observed at the GSL (Appendix B, Section 6; Fig. S8, Fig. S9, Table S8). During the study period, all datasets (except for inflows from FB) exhibited positively skewed distributions that confirmed applying a log transformation to the data as part of the PCA data processing.

### 4.2. Spatial and seasonal filters for GSL salinity data

Results from the PCA revealed the spatial patterns of south arm UBL  $S$  across seasons in response to its primary drivers (Fig. 4). Regarding seasonality, Principal Component 1 (PC1), Principal Component 2 (PC2), and Principal Component 3 (PC3) explained 72.7 % of dataset variation during runoff (RO), 73.3 % of variation during hot low-flow (HLF) months, and 62.7 % of variation during cold low-flow (CLF) months (Table 2). During RO, HLF, and CLF, the majority of UBL  $S$  observations responded similarly to PC1, PC2 and PC3. As noted in Fig. 4, data points from DWiR/USGS sites A, C, M, and N consistently deviated from the main cluster. The magnitude of  $S$  from these sites is consistently lower than other observations and occurred when river  $Q$  was higher as indicated by the 2D vector projections of  $S$  and  $Q$  in PC space (Fig. 4b; Fig. 4d; Fig. 4f). For example, the direction of the vector projections for  $S$  and  $Q$  during spring runoff (Fig. 4b) specified that the magnitude of the  $S$  observations increased from top right to bottom left while magnitude of  $Q$  increased from bottom left to top right. The outlier observations during spring runoff are clustered in the top right corner (Fig. 4b), thus these low  $S$  observations occurred when  $Q$  was high.

Additional outliers were observed during HLF and CLF that had higher  $S$  compared to the main cluster (see upper left of Fig. 4d and lower left of 4 f). These observations did not occur consistently at the same sites nor across seasons. While they may not be representative of south arm conditions, the lack of consistency in sampling location and season did not support exclusion from the representative dataset.

The compiled  $S$  time series (Fig. 5), including all available observations of UBL  $S$ , verified the patterns revealed in the PCA and showcased the general trend in UBL  $S$  influenced by the New Breach for the period of analysis. DWiR/USGS sites A, C, M, and N

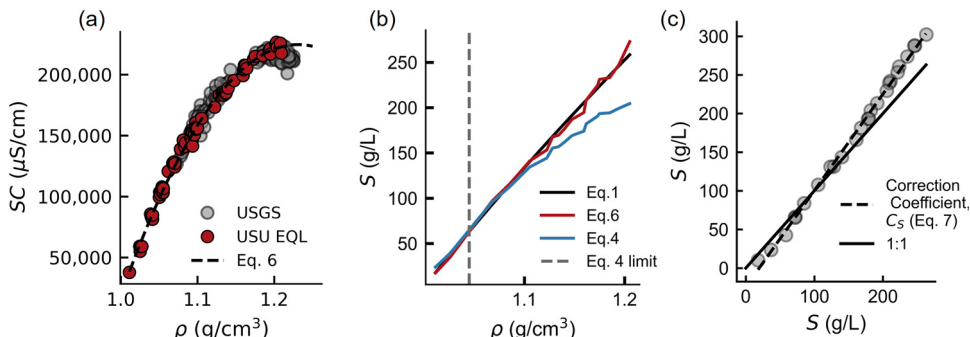


**Fig. 3.** USU-UWRL experiment results showing (a)  $\rho$  versus  $SC$  including USGS data pairs collected from the New Breach, (b) comparison of the  $S$  conversion methods, and (c)  $S$  derived from  $\rho$  versus  $S$  derived from  $\%S$ .

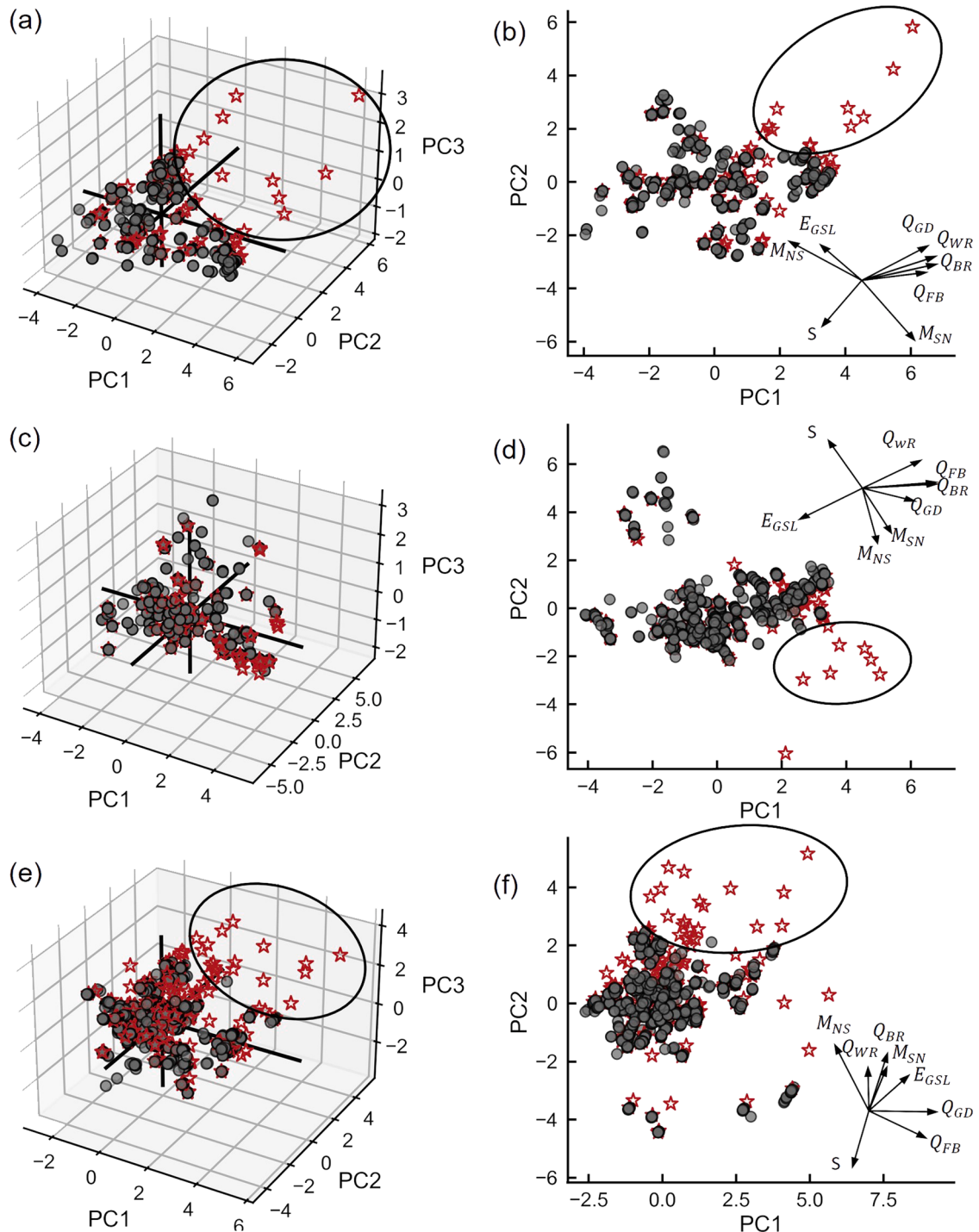


**Fig. 4.** Principal components for discrete measurements of south arm UBL  $S$  paired with daily values of  $E_{GSL}$ ,  $M_{SN}$ ,  $M_{NS}$ ,  $Q_{BR}$ ,  $Q_{WR}$ ,  $Q_{FB}$ ,  $Q_{GD}$  during (a,b) spring runoff between March and June, (c,d) hot low flow between July and October and (e,f) cold low flow between November and February. Gray circular symbols represent data from sites that were found to be representative of south arm conditions and red star symbols represent data from sites A, C, M, and N that were not included in calculating the representative UBL  $S$  time series. Observations of lower UBL  $S$  that deviate from the main cluster are circled in black. Normalized, 2D projections of each variable in PC space are included in (b, d, f) and are offset from the origin for clarity.

**Table 2**

Principal component values for runoff, hot low-flow and cold low-flow seasons.

Months	Season	Principal Component	Explained Variance	Total (%)
3–6	Runoff (RO)	PC1	0.405	72.7
		PC2	0.199	
		PC3	0.123	
		PC1	0.38	
7–10	Hot Low-Flow (HLF)	PC2	0.249	73.3
		PC3	0.104	
		PC1	0.245	
		PC2	0.222	
11–12	Cold Low-Flow (CLF)	PC3	0.16	62.7
		PC2	0.222	

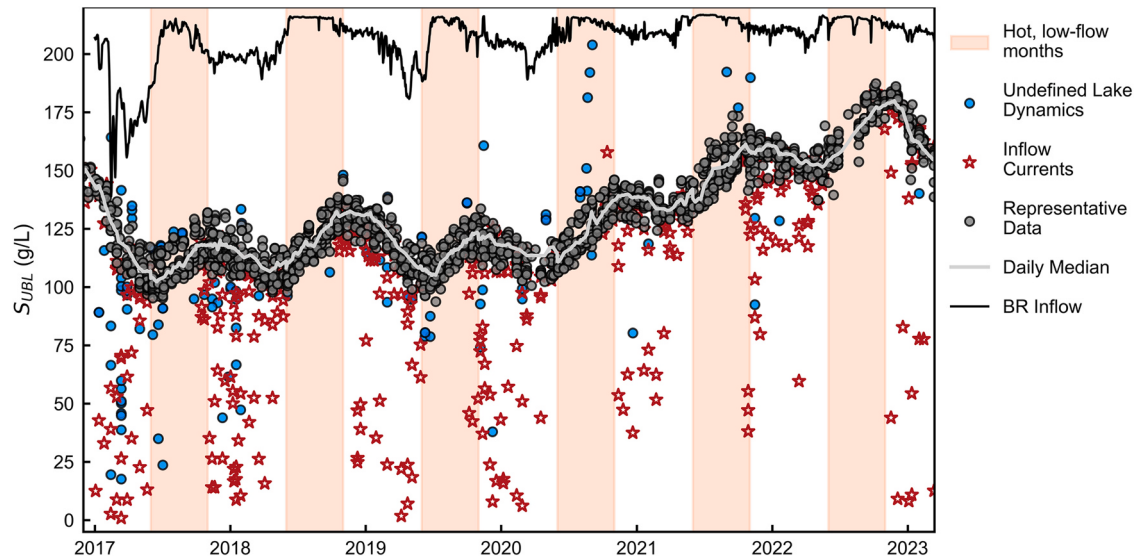


**Fig. 5.** Compiled open water  $S$  time series for the south arm UBL of the Great Salt Lake from January 2017 to December 2022. Observations from sites A, C, M, N are indicated by the red stars while remaining outlier observations are indicated by the blue dots.  $Q$  data from the Bear River at Corinne, UT (USGS 10126000) is plotted along the top.

reported significantly lower  $S$  values during the RO and CLF months (Fig. 5; Fig. S10). These outliers are assumed to be due to strong freshwater currents from high runoff in the BR entering the GSL through BR Bay and the Jordan River through FB, which have been observed during USGS field data collection (U.S. Geological Survey, 2023; Appendix B, Section 7; Fig. S10). In addition, occasional outliers were observed from seven sites (O, P, Q, R, V, X). Based on results from the PCA, the compiled  $S$  time series and the

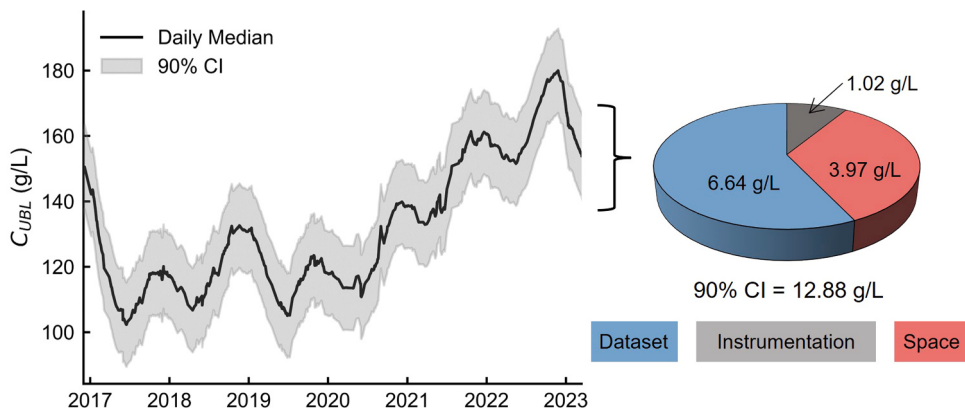


**Fig. 6.** Representative UBL  $S$  time series from January 2017 to September 2023 including the calculated 90 % confidence interval, indicated by the gray shaded region.  $\sigma$  introduced into the  $S$  dataset are from the three sources of error, which were used to calculate  $\sigma_T$  and the confidence interval.

corresponding representative south arm sampling locations identified herein, data from sites A, C, M, and N were removed from the representative GSL dataset during RO and CLF months. Remaining observations were supplemented using linear interpolation to develop daily time series at each sampling location. Daily south arm UBL  $S$  was then calculated by finding the daily median across all sites in the filtered dataset and is assumed to be representative of lake conditions when considering the south arm in its entirety (Fig. 5).

#### 4.3. Representative south arm salinity

After developing the representative UBL  $S$  series (Fig. 5), the error analysis quantified a range of uncertainty associated with combining the individual datasets, assuming spatial homogeneity across the filtered sampling locations, and instrumentation accuracy (Fig. 6; Table 3). Averaging through space and combining independent datasets contributed the most uncertainty into the representative south arm salinity time series, resulting in a spatial error source  $\sigma = 3.97 \text{ g/L}$  and dataset error source  $\sigma = 6.64 \text{ g/L}$ , respectively (Appendix B, Section 8; Fig. S11). Uncertainty due to measurement accuracy reported by the various instrument manufacturers resulted in instrumentation error  $\sigma = 1.02 \text{ g/L}$  (Appendix B, Section 8; Fig. S11). Combining the average  $\sigma$  values, the median UBL  $S$  time series is presumed to be representative of UBL conditions  $\pm 12 \text{ g/L}$  on any given day (Fig. 6).

#### 4.4. Seasonal salinity drivers

Seasonal correlation between UBL  $S$  and  $E_{GSL}$ , New Breach  $M$ , and river  $Q$  revealed which factors have a direct relationship with changes in  $S$  within the GSL (Table 4; Fig. 7). If the Theil-Sen slope 95 % confidence intervals ( $p$ -value = 0.05) did not include zero, the correlation was determined to be significant. There was a significant, negative correlation with  $Q_{BR}$ ,  $Q_{WR}$ , and  $Q_{GD}$  during RO and CLF showcasing the role river  $Q$  plays in dilution or lowering  $S$  of the south arm.  $M_{NS}$  exhibited a significant, positive correlation during CLF exemplifying the influence  $Q_{NS}$  has on raising salinity of the south arm during this period of the year, whereas it exhibited a negative correlation during HLF.  $M_{SN}$  showed significant, positive correlations during HLF and CLF despite it being the main mechanism for mass export from the south arm to the north arm (i.e.,  $Q_{SN}$ ). Additionally, neither  $M_{NS}$  nor  $M_{SN}$  exhibited significant correlation during RO, indicating that river inflows more directly influence salinity over short time scales compared to mass exchange during periods of high river inflow.

$E_{GSL}$  exhibited significant, negative correlation during HLF and CLF (Fig. 7; Table 4) despite it being the only freshwater “outflow”. During HLF, water surface elevation decreased while  $S$  within the south arm increased because  $E_{GSL}$  outweighed  $Q$  from the rivers, as exhibited by the highest  $E_{GSL}$  values occurring when  $Q$  was lowest (Fig. 8; Fig. S9b). However, the highest values of  $E_{GSL}$  occurred at the beginning of the period when  $T$  was warmest, therefore the largest values of  $E_{GSL}$  were paired with the lowest values of  $S$  explaining the negative correlation. During CLF,  $0 \leq E_{GSL} \leq 50 \text{ m}^3/\text{s}$  and were outweighed by total river  $Q$  that rarely dropped below  $30 \text{ m}^3/\text{s}$ , resulting in an increase in lake level (Fig. 8; Fig. S9b). Inflow volume outweighed  $E_{GSL}$  at the beginning of RO, but the balance was shifted toward  $E_{GSL}$  as temperatures started to rise in May, represented by the declining lake level between May and September (Fig. 8b; Fig. S9b). These results show that GSL water elevations are primarily driven by river  $Q$  during CLF and the first half of RO and driven by  $E_{GSL}$  during the second half of RO and the HLF season.

Although the seasonal correlation analysis showed no significant direct relationship between New Breach mass flux and UBL  $S$ , over longer periods,  $M_{SN}$  and  $M_{NS}$  do influence the total salt mass in the UBL, which in turn affects the relationship between lake level and  $S$  (Fig. 9). After the New Breach was opened with the submerged berm at elevation 1275 m, the south to north flows dominated with  $25.2 \text{ m}^3/\text{s} \leq Q_{SN} \leq 96.8 \text{ m}^3/\text{s}$  due to the higher WSE in the south arm (Dunn, 2025; Fig. S9). This reduced the salt mass entering the DBL from the north arm and increased salt mass leaving the UBL, leading to less  $S$  for a given lake elevation (Fig. 9). After 2022, there was no noticeable change in the total salt mass once the berm was raised to elevations of 1276.2 m and 1277.7 m, which highlights the need for longer time frames to observe and manage significant  $S$  changes.

**Table 3**  
Average standard deviation resulting from each source of uncertainty within the UBL  $S$  time series.

Source of Uncertainty	Entity	Data Subset	$\sigma$ (g/L)
Instrumentation accuracy	BSC	YSI 556 Conductivity Meter	1.02
	HDR, UGS, USGS	Anton Paar DMA 35 Density Meter	
	DwiR	Atago Master S28α Refractometer	
Averaging through space	BSC	SC	3.97
	HDR, UGS, USGS	$\rho$	
Combining multiple datasets	DWiR	%S	6.64
	BSC, UGS, USGS	GSL site 3510 GSL site 2565	

\*Note:  $\sigma$  is the average standard deviation from each type of error in the representative UBL  $S$  dataset, calculated from the daily standard deviation time series.

**Table 4**

Theil Sen slopes and corresponding 95 % confidence intervals between  $S$  and each variable included within the PCA.

Variable	RO		HLF		CLF	
	Slope	95 % CI	Slope	95 % CI	Slope	95 % CI
$E_{GSL}$	3.02	[− 3.28, 10.68]	<b>− 4.17</b>	[− 5.83, − 2.80]	<b>− 14.12</b>	[− 20.51, − 8.98]
$M_{NS}$	5.13	[− 3.59, 13.03]	<b>− 2.23</b>	[− 3.64, − 0.86]	<b>12.48</b>	[9.84, 14.8]
$M_{SN}$	− 7.68	[− 18.54, 1.69]	<b>4.22</b>	[2.88, 5.50]	5.12	[3.50, 6.77]
$Q_{BR}$	<b>− 13.44</b>	[− 20.40, − 5.68]	1.11	[− 4.35, 4.71]	<b>− 6.67</b>	[− 8.57, − 4.55]
$Q_{WR}$	<b>− 27.99</b>	[− 44.71, − 6.71]	<b>6.69</b>	[4.25, 8.95]	<b>− 20.94</b>	[− 24.47, − 17.71]
$Q_{GD}$	− 2.72	[− 13.96, 10.42]	<b>− 3.21</b>	[− 5.21, − 1.13]	<b>− 22.22</b>	[− 51.64, − 6.75]
$Q_{FB}$	2.41	[− 6.71, 11.38]	<b>4.93</b>	[1.31, 8.23]	<b>− 9.94</b>	[− 13.33, − 6.60]

Note: Slopes that are bolded indicate a significant ( $p$  value < 0.05) linear relationship between log-transformed data.

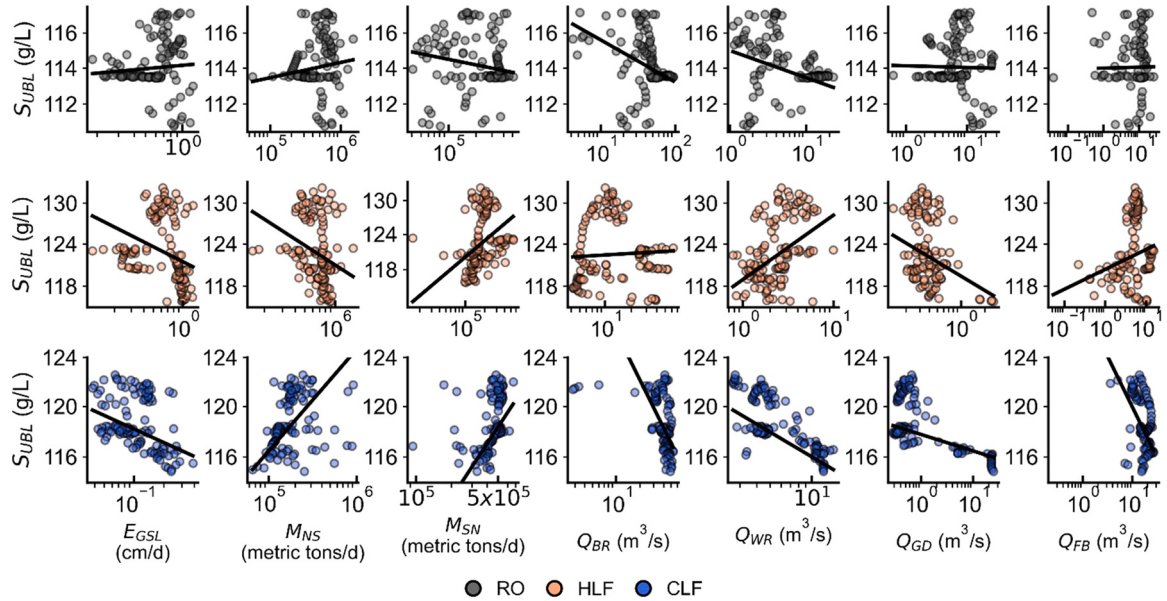


**Fig. 7.** Representative UBL  $S$  plotted against evaporation, New Breach salt fluxes, and river inflows from October 2019 to September 2020, separated and colored by season. Solid black lines indicate Theil Sen regression lines. RO refers to spring runoff months between March and June, HLF refers to hot, low river inflow months between July and October, and CLF refers to cold, low river inflow months between November and February.

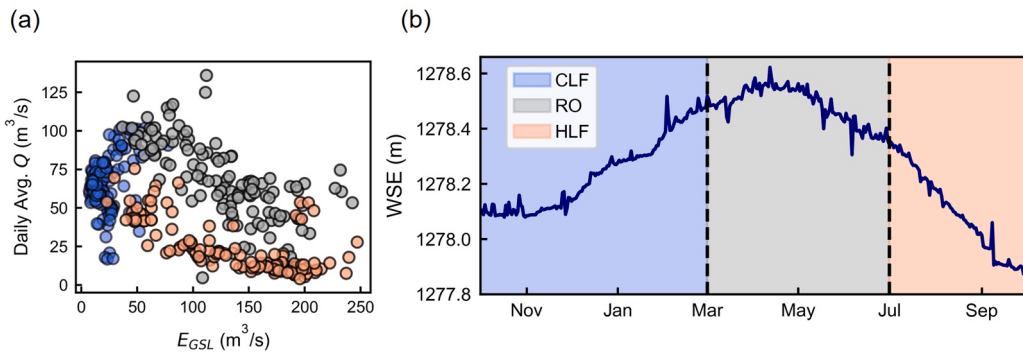


**Fig. 8.** Total, average daily river  $Q$  to the GSL plotted against  $E_{GSL}$  (a) and south arm WSE time series (b) from October 2019 to October 2020.

## 5. Discussion

During this study, new methods were developed to combine and integrate all post-New Breach disparate  $S$  data into a comprehensive daily dataset, revealing that the majority of sampling locations provide representative  $S$  values of the UBL during most of the

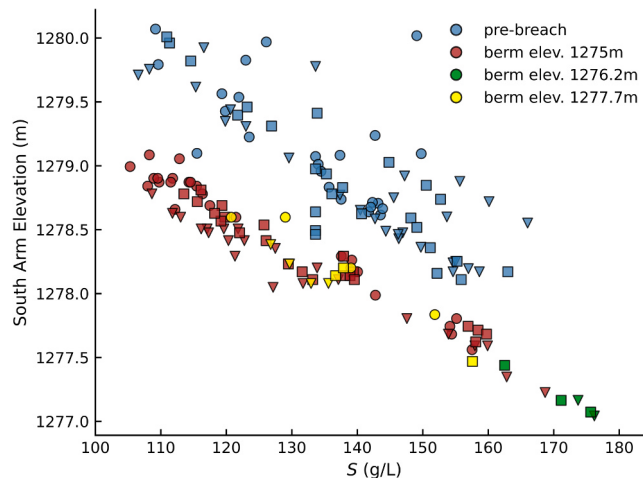


**Fig. 9.** Monthly average representative UBL  $S$  compared to south arm WSE from 2011 to 2023, colored by New Breach berm elevation. Triangles indicate measurements taken during hot low flow seasons, circles indicate runoff season measurements, and squares indicate cold low flow season measurements.

year. The accuracy of this daily time series could be improved, particularly for the DBL, with more frequent monitoring and with increased spatial extents. However, despite the uncertainties quantified in this study, this new daily  $S$  dataset provides a general understanding of how the south arm UBL seasonally fluctuates and how it is affected by GSL watershed hydrology and lake management decisions. This time series combined with streamflow, evaporation, and New Breach mass flux data can inform future GSL management decisions.

### 5.1. Daily GSL Data implications

#### 5.1.1. Available salinity data usage

$S$  conversion methods documented herein facilitate the continued compilation of all future  $S$  datasets derived from multiple water quality parameters. Analysis of Eq. (4) validated expanded usage of the AWWA SC conversion method to 100 g/L. However, performance of the newly developed Eq. (6) favors implementation for converting open water SC to  $S$  and for saline lakes of similar ion composition and concentration. Of all the available datasets, % $S$  measurements were taken at the highest temporal resolution, but were shown to overpredict  $S$  compared to other proxy measurements. The newly developed Eq. (6) and  $C_{\%S}$  conversion factor allows comparison to  $S$  estimated from other proxy measurements. While analysis of the GSL EOS (Eq. (1)) was not performed, it has previously been determined applicable for GSL south arm waters (Great Salt Lake Salinity Advisory Committee, 2020a, 2020b) and may be valid for north arm  $\rho$  measurements (confirmation recommended).

Utilizing these methods, this study developed the highest spatial and temporal resolution  $S$  data available for the GSL beginning in 2017 with the New Breach. This new daily time series offers a more detailed understanding of historical UBL  $S$  conditions and is more conducive to salt-mass balance modeling and capturing the daily and seasonal lake dynamics. Thus, the effects of recent berm modifications can be more appropriately considered and management decisions better informed by increased data.

#### 5.1.2. Salinity monitoring improvements

While the daily  $S$  time series was found to be representative of GSL UBL conditions within reasonable error ( $\pm 12$  g/L), sources of error quantified herein highlight viable monitoring improvements to better understand lake dynamics and decrease measurement uncertainties. Specifically, uncertainty due to sampling frequency could not be evaluated due to the lack of temporal data; the results of this study highlight the need for  $S$  data sampled at least every two weeks. Additionally, new insight into  $S$  mixing patterns such as currents within the DBL, observed by Naftz (2014), and UBL/DBL mixing events triggered by high wind may be found if sampling frequency at all monitoring sites were to increase. To overcome challenges associated with more frequent  $S$  sampling, coordination between the various entities is recommended, which was also proposed to all monitoring entities by the GSL Salinity Advisory Committee (2020b).

#### 5.1.3. Additional monitoring needs

Improved monitoring of other hydrologic variables at the GSL is also needed. Current estimates for the BR and WR are insufficient due to significant geographical challenges. River inflows were one of the biggest influences on UBL  $S$ , yet high uncertainties currently exist with the BR and WR stream gages. The WR gage is upstream from the Ogden Bay Waterfowl Management Area, a 20,000-acre wetland. Similarly, the BR gage at Corinne is about 42 km northwest of the BR Bay Bridge and is upstream of the BR Migratory Bird Refuge and the BR Bay which is flanked by mineral evaporation ponds. More accurate monitoring of river  $Q$  values (tracking sinks, sources, and storage of water and salt in wetlands) should be prioritized due to their proven significance. Continuous monitoring of  $Q$

and SC at the BR Bay Bridge, like the FB Bridge, would allow for better estimation of water inflows and salt loading from GSL's main tributary. Monitoring of the exchange flows at the New Breach should also be measured at a similar temporal frequency to river inflows to allow the predictive DNN and GABI models to be used for forecasting or to accommodate future berm modifications. Finally, limited information is available regarding mineral extraction activities and corresponding  $S$  and  $Q$  of brine pumped and occasionally returned to the GSL.  $E_{GSL}$  is also not monitored; therefore, the calculation method developed by [Mohammed and Tarboton \(2012\)](#) cannot be verified using direct measurements. This introduces uncertainty into estimates of this variable which would be rectified if field data was available.

### 5.2. GSL salinity controls

Results from the correlation analysis and comparison of  $E_{GSL}$  and river  $Q$  revealed which  $S$  controls are influential at a seasonal scale. UBL  $S$  is inversely related to the interannual variation in lake elevation which is dictated by the balance between evaporation and river inflows. While  $E_{GSL}$  was not found to be directly correlated with UBL  $S$ , seasonal daily estimates demonstrate that it is the primary driver of decreasing south arm lake elevations during the second half of RO and HLF.  $E_{GSL}$  cannot be reduced, thus increasing streamflow to the lake during these seasons is imperative to maintain a healthy lake volume.

$M_{SN}$  is the main mechanism for salt mass export from the UBL but was not significantly correlated to UBL  $S$  at a seasonal scale. Instead, reducing  $S$  in the south arm via  $M_{SN}$  occurred at an interannual time scale (see [Fig. S9](#)). However, altering  $M_{NS}$  can more rapidly affect south arm  $S$  as it is directly responsible for DBL formation and persistence. During periods where the DBL exists, the UBL receives mass from the DBL due to turbulent diffusion across the layer interface. Further, mass is also transferred to the UBL during GSL high wind mixing events ([Wurtsbaugh and Jones, 2014](#); [Naftz et al., 2014](#)). Without the presence of  $M_{NS}$ , the DBL was observed to dissipate into the UBL within 6 months ([Yang et al., 2020](#)), emphasizing the role that  $M_{NS}$  plays in supplying the DBL with salt mass which is transferred to the UBL and immediately impacts UBL  $S$ .

Given the interdependent relationships between  $Q$  at the New Breach, river  $Q$ ,  $E_{GSL}$ , and  $S$ , the linear correlation analysis performed herein is not fully equipped to evaluate management strategies. Further, the exchange flow models employed in this study are limited to the current New Breach geometry. Therefore, to aid future management decisions, there is a clear need for mechanistic modeling of the New Breach that can predict  $M_{NS}$  and  $M_{SN}$  for varying New Breach geometries and can be incorporated into a process-based lake model that accurately predicts lake elevation and  $S$  for future drought-flood cycles and berm alterations.

### 5.3. Management implications

Results from this study reiterate that GSL is a complex, dynamic system. Despite challenges in isolating the controls of  $S$ , some effective strategies emerged. River  $Q$  was directly correlated with decreasing UBL  $S$ , thus increasing streamflow to the lake is paramount to prevent repetition of the record low GSL elevations and high  $S$  experienced in 2022. Additionally, changes to New Breach mass flux via alterations to berm height can be used to adapt to extreme conditions such as the raise in 2023 that trapped all freshwater inflows in the south arm and returned the UBL  $S$  to healthy levels. In the long term, the berm could be adjusted as needed each year to slowly change the distribution of salt mass within the lake. However, because of the complexity of the UBL and DBL interactions and the impact on UBL salinity, the tools to fully understand the implications of berm alterations do not currently exist and the berm itself does not provide full control of the exchange flows to managers. A lake wide mass balance model that accounts for DBL and UBL dynamics and incorporates additional modeling tools that capture complex bi-directional flows at the New Breach would fill this gap. Such tools could be used to establish streamflow requirements and annual exchange flows that meet elevation/salinity goals at multiple time scales.

## 6. Conclusion

Following the opening of the New Breach in the causeway at the Great Salt Lake, all available  $S$  related measurements from various agencies were combined and a daily  $S$  dataset was produced for the GSL. This required a new method for converting SC to  $S$  and a % $S$  adjustment factor.  $S$  across open water sampling locations was spatially and seasonally filtered and data uncertainty was quantified, resulting in daily median values across sampling locations with errors of  $\pm 12$  g/L. Seasonal influence of key GSL inflows and outflows were also determined through correlation analysis. A new method for predicting the north-to-south and south-to-north exchange  $Q$  at the New Breach was incorporated; flows through the New Breach influenced south arm  $S$ , however, fluctuations in the balance between river  $Q$  and  $E_{GSL}$  were the main drivers of  $S$ . Based on these results, the implications of this dataset highlight the need for more frequent and increased spatial monitoring at the GSL and continued coordination of sampling methods. The understanding of GSL  $S$  could also be improved by more accurately tracking  $Q$  data through the New Breach and the Bear River Bay Bridge, groundwater contributions, salt export from mineral extraction activities, and validation of the current GSL evaporation estimation method.

As conditions at the lake continue to evolve in response to anthropogenic and environmental stressors, there is an immediate need to determine the most effective means to adaptively manage salt concentrations. Because lake elevation and  $S$  is a function of multiple, interdependent hydrologic variables, the most commonly used tool to inform management actions is modeling, which requires data at appropriate spatial and temporal scales. Increasing  $S$  sampling frequency, diminishing uncertainty in combining multiple datasets, and accurately tracking key inflows/outflows including a GSL specific evaporation model would significantly aid future modeling efforts and sustainable salinity management at the GSL.

These findings more broadly impact research throughout the GSL drainage area and adjacent metropolitan regions including water

diversions, health risks associated with exposed lakebed, GSL ecology and adjacent wetlands, groundwater and seepage, instrumentation in harsh brine environments, and similar efforts at other terminal salt lakes throughout the globe.

### CRediT authorship contribution statement

**Phillips Colin:** Writing – review & editing, Methodology, Formal analysis. **Crookston Brian:** Writing – review & editing, Writing – original draft, Visualization, Validation, Supervision, Software, Resources, Project administration, Methodology, Investigation, Funding acquisition, Formal analysis, Data curation, Conceptualization. **Dunn Diana:** Writing – review & editing, Writing – original draft, Visualization, Validation, Software, Methodology, Investigation, Formal analysis, Data curation, Conceptualization. **Neilson Bethany:** Writing – review & editing, Visualization, Validation, Methodology, Investigation, Formal analysis, Data curation, Conceptualization. **Dutta Som:** Writing – review & editing, Methodology, Formal analysis.

### Supporting Information

Supplemental information associated with this article can be found in the online version at doi:10.1016/j.ejrh.2025.102332.

### Declaration of Competing Interest

The authors declare that they have no known competing financial interests or personal relationships that could have appeared to influence the work reported in this paper.

We also declare that:

- the work described has not been published previously except in the form of an academic thesis.
- the article is not under consideration for publication elsewhere.
- the article's publication is approved by all authors and tacitly or explicitly by the responsible authorities where the work was carried out.

We also declare that:

- if accepted, the article will not be published elsewhere in the same form, in English or in any other language, including electronically, without the written consent of the copyright-holder.

### Acknowledgements

This study was funded by the State of Utah through the Department of Natural Resources—Forestry, Fire and State Lands and the Utah Water Research Laboratory. Special thanks to Dr. Joan McLean at the USU UWRL for their valuable expertise and assistance in performing the experiment in the USU UWRL EQL.

### Appendix A. Great Salt Lake inflow and climate data sources

**Table A1**

Great Salt Lake inflow and causeway exchange data sources used to calculate New Breach exchange and inflow volume.

Entity	Site	ID	Lat	Lon	$Q_D$ (cfs)	$Q_C$ (cfs)	$SC_D$ (uS/cm)	$SC_C$ (uS/cm)	$\rho_D$ (g/cm <sup>3</sup> )
USGS	Bear River near Corinne, UT	10126000	41.58	− 112.85	✓	✓	✓	✓	✓
	Weber River at Plain City, UT	10141000	41.28	− 112.09	✓	✓	✓	✓	✓
	Goggin Drain	10172630	40.82	− 112.10	✓	✓	✓	✓	✓
	Farmington Bay	41040112134801	41.07	− 112.23	✓	✓	✓	✓	✓
	WCB SN Flow	10010025	41.22	− 112.77	✓		✓		✓
	WCB NS Flow	10010026	41.22	− 112.77	✓		✓		✓
USU	WCB South	−	41.22	− 112.77			✓		✓
	WCB North	−	41.22	− 112.77			✓		✓
HDR	SN Flow	−	41.22	− 112.77			✓		✓
	NS Flow	−	41.22	− 112.77			✓		✓

Note: "C" subscript represents 15-minute continuous measurements while "D" subscript represents discrete measurements.

**Table A2**

Great Salt Lake climate data sources used to calculate evaporation off the Great Salt Lake.

Entity	Site	Lat	Lon	Elevation (ft)	$v_w$ (mph)	P (mbar)	$T_{max}$ , $T_{min}$ (F)	WSE (ft)	Frequency
UCC	Hat Island	41.33	-112.85	4242.13	✓	✓	✓ ✓	Hourly	Hourly
	Gunnison Island	41.07	-112.59	4242.13	✓	✓	✓ ✓		
	MARSH	41.22	-112.67	4212.93	✓	✓	✓ ✓		
USGS	10010025	41.22	-112.77	4216.93	✓				15-min

**Appendix B. Supporting information**

Supplementary data and information associated with this article can be found in the online version at doi:[10.1016/j.ejrh.2025.102332](https://doi.org/10.1016/j.ejrh.2025.102332).

**Data availability**

All data that support the findings of this study are publicly accessible, available at <https://doi.org/10.4211/hs.438b751c1ff84555a36592345fcfa6b7>.

**References**

- Barnes, B.D., Wurtzbaugh, W.A., 2015. The effects of salinity on plankton and benthic communities in the Great Salt Lake, Utah, USA: a microcosm experiment. *Can. J. Fish. Aquat. Sci.* 72 (6), 807–817. <https://doi.org/10.1139/cjfas-2014-0396>.
- Bioeconomics, Inc, 2012. *Economic Significance of the Great Salt Lake to the State of Utah*. Prepared for the State of Utah Great Salt Lake Advisory Council, Salt Lake City, Utah.
- Brown, P.D., Bosteels, T., Marden, B.T., 2023. Salt load transfer and changing salinities across a new causeway breach in Great Salt Lake: implications for adaptive management. *Lakes Reserv.: Sci. Policy Manag. Sustain. Use* 28 (1). <https://doi.org/10.1111/lre.12421>.
- Brown, P.M.B.L.C., Hambley, D.F., 2002. Statistics for environmental engineers. *Environ. Eng. Geosci.* 8 (3), 244–245. <https://doi.org/10.2113/8.3.244>.
- Chapra, S.C., 1997. *Surface Water Quality Modeling*. McGraw-Hill Publisher, New York.
- Donnelly, J.P., King, S.L., Silverman, N.L., Collins, D.P., Carrera-Gonzalez, E.M., Lafón-Terrazas, A., Moore, J.N., 2020. Climate and human water use diminish wetland networks supporting continental waterbird migration. *Glob. Change Biol.* 26 (4), 2042–2059. <https://doi.org/10.1111/gcb.15010>.
- Dunn, D.G., 2024. A Mass Balance Model of the Great Salt Lake, UT with Adaptive Management Applications. Thesis. Utah State University. (<https://digitalcommons.usu.edu/etd2023/350/>).
- Dunn, D. Great Salt Lake Salinity, Climate, and Inflow Data, HydroShare. <http://www.hydroshare.org/resource/438b751c1ff84555a36592345fcfa6b7>.
- ECONorthwest, 2019. Assessment of Potential Costs of Declining Water Levels in Great Salt Lake. (<https://documents.deq.utah.gov/water-quality/standards-technical-services/great-salt-lake-advisory-council/activities/DWQ-2019-012913.pdf>).
- Great Salt Lake Salinity Advisory Committee, 2020a. Round Robin of Methods to Estimate the Salinity of Great Salt Lake Waters. Utah Geological Survey. (<https://doi.org/10.34191/OFR-427>).
- Great Salt Lake Salinity Advisory Committee, 2020b. Standard Operating Procedure—Great Salt Lake Water Density Measurement and Salinity Calculation. Utah Geological Survey. <https://doi.org/10.34191/OFR-728>.
- Great Salt Lake Salinity Advisory Committee, 2021. Influence of Salinity on the Resources and Uses of Great Salt Lake. Utah Geological Survey. <https://doi.org/10.34191/OFR-736>.
- Great Salt Lake Strike Team, 2023. Great Salt Lake Policy Assessment: A Synthesized Resource Document for the 2023 General Legislative Session. (<https://gardner.utah.edu/wp-content/uploads/GSL-Assessment-Feb2023.pdf?x71849>).
- Great Salt Lake Strike Team, 2024. Great Salt Lake Data and Insights Summary: A Synthesized Resource Document for the 2024 General Legislative Session. (<https://d36oiwf74r1rap.cloudfront.net/wp-content/uploads/2024/01/GSL-Insights-Summary-Jan2024.pdf>).
- Gwynn, J.W., Sturm, P.A., 1986. Effects of Breaching the Southern Pacific Railroad Causeway, Great Salt Lake Utah-Physical and Chemical Changes August 1, 1984–July. Utah Geol. Miner. Surv. [https://ugspub.nr.utah.gov/publications/water\\_resources/bulletins/wrb-25.pdf](https://ugspub.nr.utah.gov/publications/water_resources/bulletins/wrb-25.pdf).
- HDR Engineering, Inc, 2014. Union Pacific Railroad Great Salt Lake Causeway Culvert Closure and Bridge Construction Project, Bridge Evaluation Report. Utah Department of Environmental Quality. (<https://documents.deq.utah.gov/water-quality/standards-technical-services/gsl-website-docs/delete/DWQ-2019-000480.pdf>).
- Helsel, D.R., Hirsch, R.M., Ryberg, K.R., Archfield, S.A., Gilroy, E.J., 2020. Statistical Methods in Water Resources: U.S. Geological Survey Techniques and Methods, book 4, chapter A3, 458 p. [Supersedes USGS Techniques of Water-Resources Investigations, book 4, chapter A3, version 1.1]. (<https://doi.org/10.3133/tm4a3>).
- Horsburgh, J.S., Jones, A.S., Black, S.S., Hodson, T.O., 2022. USGS data retrieval python package usage examples. HydroShare. (<http://www.hydroshare.org/resource/c97c32ecf59b4dff90ef013030c54264>).
- Jewell, P.W., 2021. Historic low stand of Great Salt Lake, Utah: I: mass balance model and origin of the deep brine layer. *SN Appl. Sci.* 3 (8), 757. <https://doi.org/10.1007/s42452-021-04691-5>.
- Larsen, E., 2024. Rapid Prediction of Buoyancy-Driven Exchange Flows at the Great Salt Lake: ML Models and a 1D Shallow Water Approach (Thesis). Utah State University. (<https://digitalcommons.usu.edu/etd2023/319/>).
- Levesque, V.A., Oberg, K.A., 2012. Computing discharge using the index velocity method. *U. S. Geol. Surv. Tech. Methods* 3–A23, 148. (<https://pubs.usgs.gov/tm/3a23/>).
- Lindsay, M.R., Johnston, R.E., Baxter, B.K., Boyd, E.S., 2019. Effects of salinity on microbialite-associated production in Great Salt Lake Utah. *Ecol. Soc. Am.* 100 (3). <https://doi.org/10.1002/ecy.2611>.
- Madison, R.J., 1970. Effects of a causeway on the chemistry of the brine in Great Salt Lake Utah. *Water Resour. Bull.* 14. ([https://ugspub.nr.utah.gov/publications/water\\_resources\\_bulletins/WRB-14.pdf](https://ugspub.nr.utah.gov/publications/water_resources_bulletins/WRB-14.pdf)).
- Marden, B., Brown, P., Bosteels, T., 2020. Great salt lake artemia: ecosystem functions and services with a global reach. In: Baxter, In.B.K., Butler, J.K. (Eds.), *Great Salt Lake Biology*. Springer International Publishing, pp. 175–237. [https://doi.org/10.1007/978-3-030-40352-2\\_7](https://doi.org/10.1007/978-3-030-40352-2_7).
- McIlwain, H.E., Arias, M.C., McDonnell, M.C., Seawolf, S.M., Rumsey, C.A., 2023. Vertical Water-quality Profiles Collected at Great Salt Lake Monitoring Sites, Utah, 1995–2022. U.S. Geological Survey data release. <https://doi.org/10.5066/P9J6A07X>.
- Merck, M.F., Tarboton, D.G., 2023. The salinity of the Great Salt Lake and its deep brine layer. *Water* 15 (8), 1488. <https://doi.org/10.3390/w15081488>.

- Mohammed, I.N., 2006. Modeling the Great Salt Lake. Thesis. Utah State University. ([https://hydrology.usu.edu/dtarb/ibrahim\\_thesis.pdf](https://hydrology.usu.edu/dtarb/ibrahim_thesis.pdf)).
- Mohammed, I.N., Tarboton, D.G., 2012. An examination of the sensitivity of the Great Salt Lake to changes in inputs: great salt lake sensitivity index. Water Resour. Res. 48 (11). <https://doi.org/10.1029/2012WR011908>.
- Naftz, D.L., Carling, G.T., Angeroth, C., Freeman, M., Rowland, R., Pazmiño, E., 2014. Density-stratified flow events in Great Salt Lake, Utah, USA: implications for mercury and salinity cycling. Aquat. Geochem. 20 (6), 547–571. <https://doi.org/10.1007/s10498-014-9237-8>.
- Naftz, D.L., Millero, F.J., Jones, B.F., Reed Green, W., 2011. An equation of state for hypersaline water in Great Salt Lake, Utah, USA. Aquat. Geochem. 17 (6), 809–820. <https://doi.org/10.1007/s10498-011-9138-z>.
- Null, Wurtsbaugh, Miller, W., C, 2013. Can the causeway in the Great Salt Lake be used to manage salinity? Friends Gt. Salt Lake Newsl. 19 (1), 14–15. ([http://works.bepress.com/wayne\\_wurtsbaugh/143/](http://works.bepress.com/wayne_wurtsbaugh/143/)), 2.
- Null, S.E., Wurtsbaugh, W.A., 2020. Water development, consumptive water uses, and Great Salt Lake. In: Baxter, B., Butler, J. (Eds.), Great Salt Lake Biology. Springer, Cham. <https://doi.org/10.1007/978-3-030-40352-2>.
- Perry, K.D., Crozman, E.T., Hoch, S.W., 2019. Results of the Great Salt Lake Dust Plume Study (2016–2018) (Tech. Rep.). Department of Atmospheric Sciences, University of Utah. ([https://d1bbnjcim4vtri.cloudfront.net/wp-content/uploads/2019/12/10101816/GSL\\_Dust\\_Plumes\\_Final\\_Report\\_Complete\\_Document.pdf](https://d1bbnjcim4vtri.cloudfront.net/wp-content/uploads/2019/12/10101816/GSL_Dust_Plumes_Final_Report_Complete_Document.pdf)).
- Rasmussen, M., 2022. Using Computational Fluid Dynamics to Predict Flow Through the West Crack Breach of the Great Salt Lake Railroad Causeway. Thesis Utah State University. (<https://digitalcommons.usu.edu/etd/8529/>).
- Rasmussen, M.T., Dutta, S., Neilson, B.T., Crookston, B.M., 2021. CFD model of the density-driven bidirectional flows through the west crack breach in the Great Salt Lake causeway. Water 13 (17), 2423. <https://doi.org/10.3390/w13172423>.
- Schemel, L.E., 2001. Simplified conversions between specific conductance and salinity units for use with data from monitoring stations. In: Interagency Ecological Program Newsletter, 14. USGS Publications Warehouse, pp. 17–18. (<https://pubs.usgs.gov/publication/70174311>).
- Spieweck, F., Bettin, H., 1992. Review: solid and liquid density determination. Technisches Messen, vol. 59, pp. 285–92. doi: 10.1524/teme.1992.59.78.285.
- U.S. Geological Survey, 2002. Processing of Water Samples (ver. 2.0): U.S. Geological Survey Techniques of Water-Resources Investigations, book 9, chap. A4. Accessed 1 August 2022, from (<http://pubs.water.usgs.gov/twi9A>).
- U.S. Geological Survey, 2023. National Water Information System: U.S. Geological Survey Web Interface. Accessed 10 June 2023, from (<https://doi.org/10.5066/F7P55KJN>).
- Utah Department of Water Quality, 2022. Union Pacific Railroad Great Salt Lake Permanent East Culvert Closure and Bridge construction Project. (<https://documents.deq.utah.gov/water-quality/facilities/401-wq-cert/DWQ-2022-001884.pdf>).
- Utah Geological Survey 2020. Great Salt Lake brine chemistry database: ([https://geology.utah.gov/docs/xls/GSL\\_brine\\_chem\\_db.xlsx](https://geology.utah.gov/docs/xls/GSL_brine_chem_db.xlsx)).
- Utah State University - Utah Climate Center. USU Climate Center. (<https://climate.usu.edu>). (Accessed 24 January 2024).
- Vanderplas, Jacob T., 2016 Python Data Science Handbook: Tools and Techniques for Developers. O'Reilly. (<https://jakevdp.github.io/PythonDataScienceHandbook/>).
- Wang, S.-Y., Gillies, R.R., Jin, J., Hipps, L.E., 2010. Coherence between the Great Salt Lake Level and the Pacific Quasi-Decadal Oscillation. J. Clim. 23 (8), 2161–2177. <https://doi.org/10.1175/2009JCLI2979.1>.
- White, J. S., & Null, S. E. (2015). Climate Variability Effects on Utah's Great Salt Lake with Proposed Causeway Modifications. DOI: 10.13140/RG.2.1.2164.0806.
- Williams, A.P., Cook, E.R., Smerdon, J.E., Cook, B.I., Abatzoglou, J.T., Bolles, K., Baek, S.H., Badger, A.M., Livneh, B., 2020. Large contribution from anthropogenic warming to an emerging North American megadrought. Science 368 (6488), 314–318. <https://doi.org/10.1126/science.aaz9600>.
- Wurtsbaugh, W.A., 2014. Management of the Great Salt Lake Ecosystem: Water, Economic Values and Competing Interests (Paper 594). Watershed Sciences Faculty Publications. ([https://digitalcommons.usu.edu/wats\\_facpub/594](https://digitalcommons.usu.edu/wats_facpub/594)).
- Wurtsbaugh, W.A., Jones, E.F., 2014. The Great Salt Lake's deep brine layer and its importance for mercury bioaccumulation in brine shrimp (*Artemia franciscana*). Limnol. Oceanogr. 59 (1), 141–151. <https://doi.org/10.4319/lo.2014.59.1.0141>.
- Yang, S., Johnson, W.P., Black, F.J., Rowland, R., Rumsey, C., Piskadlo, A., 2020. Response of density stratification, aquatic chemistry, and methylmercury to engineered and hydrologic forcings in an endorheic lake (Great Salt Lake, U.S.A.). Limnol. Oceanogr. 65 (5), 915–926. <https://doi.org/10.1002/lo.11358>.